Monthly Notices
of the
ROYAL ASTRONOMICAL SOCIETY

MNRAS **442,** 3711–3721 (2014) doi:10.1093/mnras/stu1095

Hierarchy and size distribution function of star formation regions in the spiral galaxy NGC 628

Alexander S. Gusev★

Sternberg Astronomical Institute, Lomonosov Moscow State University, Universitetsky pr. 13, 119992 Moscow, Russia

Accepted 2014 June 2. Received 2014 June 2; in original form 2013 December 24

ABSTRACT

Hierarchical structures and the size distribution of star formation regions in the nearby spiral galaxy NGC 628 are studied over a range of scales from 50 to 1000 pc using optical images obtained with the 1.5-m telescope of the Maidanak Observatory. We have found hierarchically structured concentrations of star formation regions in the galaxy, and smaller regions with a higher surface brightness are located inside larger complexes that have a lower surface brightness. We illustrate this hierarchy using a dendrogram, or structure tree, of the detected star formation regions, which demonstrates that most of these regions are combined into larger structures over several levels. We have found three characteristic sizes of young star groups: ≈65 pc (OB associations), ≈240 pc (stellar aggregates) and ≈600 pc (star complexes). The cumulative size distribution function of star formation regions is found to be a power law with a slope of approximately −1.5 on scales appropriate to diameters of associations, aggregates and complexes. This slope is close to the slope found earlier by B. Elmegreen et al. for star formation regions in the galaxy on scales from 2 to 100 pc.

Key words: H II regions – galaxies: individual: NGC 628 (M74).

1 INTRODUCTION

As is known, physical processes such as gravitational collapse and turbulence compression play a key role in the creation and evolution of star formation regions over a wide range of scales, from star complexes to OB associations down to compact embedded clusters and to clumps of young stars inside these. These stellar systems form a continuous hierarchy of structures for all these scales (Efremov 1995; Efremov & Elmegreen 1998; Elmegreen et al. 2000; Elmegreen 2002, 2006, 2011). It is suggested that the hierarchy extends up to 1 kpc (Efremov, Ivanov & Nikolov 1987; Elmegreen & Efremov 1996; Zhang, Fall & Whitmore 2001).

Efremov et al. (1987) and Ivanov (1991) have described at least three categories of hierarchical star groups on the largest levels: OB associations with a length-scale ≈80 pc, stellar aggregates with a length-scale ≈250 pc and star complexes with diameters ≈600 pc. H I/H_2 superclouds are ancestors of star complexes, and OB associations are formed from giant molecular clouds (Efremov 1989, 1995; Elmegreen 1994, 2009; Elmegreen & Efremov 1996; Efremov & Elmegreen 1998; Odekon 2008; de la Fuente Marcos & de la Fuente Marcos 2009). The sizes and clustering of these structures have been studied for many nearby spiral and irregular galaxies (Feitzinger & Braunsfurth 1984; Battinelli 1991; Wilson 1991, 1992; Magnier et al. 1993; Battinelli, Efremov & Magnier 1996; Bresolin, Kennicutt & Stetson 1996; Bresolin et al. 1998; Harris & Zaritsky 1999; Elmegreen & Elmegreen 2001; Pietrzyński et al. 2001, 2005; Gusev 2002; Borissova et al. 2004; Bastian et al. 2005; Gouliermis et al. 2010; Sánchez et al. 2010; Bruevich, Gusev & Guslyakova 2011; Bianchi et al. 2012). The power-law power spectra of optical light in galaxies suggest the same maximum scale, possibly including the ambient galactic Jeans length (Elmegreen, Elmegreen & Leitner 2003a; Elmegreen et al. 2003b). If the ambient Jeans length is the largest scale, then a combination of gravitational and turbulent fragmentations can drive the whole process. Observed star formation rates in galaxies can follow from such turbulent structures (Krumholz & McKee 2005).

Hierarchical clustering disappears with age as stars mix. The densest regions have the shortest mixing times and lose their substructures first. Nevertheless, very young clusters have a similar pattern of subclustering, suggesting that this structure continues down to individual stars (Heydari-Malayeri et al. 2001; Brandeker, Jayawardhana & Najita 2003; Kumar, Kamath & Davis 2004; Dahm & Simon 2005; Oey et al. 2005; Sánchez-Monge et al. 2013).

The interstellar matter also shows a hierarchical structure from the largest giant molecular clouds down to individual clumps and cores. The complex hierarchical structure of the interstellar matter is shaped by supersonic turbulence (Ballesteros-Paredes et al. 2007). The scaling relations observed in molecular clouds (Larson 1981) can be explained by the effect of turbulence, where energy is injected at largest scales and cascades down to the smallest scales, creating eddies and leading to a hierarchical structure on all scales

★ E-mail: gusev@sai.msu.ru

Table 1. Basic parameters of NGC 628.

Parameter	Value
Type	Sc
RA (J2000.0)	$01^{h}36^{m}41\overset{s}{.}81$
Dec. (J2000.0)	$+15^{\circ}47'00\overset{''}{.}3$
Total apparent B magnitude (B_t)	9.70 mag
Absolute B magnitude (M_B)[a]	−20.72 mag
Inclination (i)	7°
Position angle (PA)	25°
Apparent corrected radius (R_{25})[b]	5.23 arcmin
Apparent corrected radius (R_{25})[b]	10.96 kpc
Distance (D)	7.2 Mpc

[a]Absolute magnitude of a galaxy corrected for Galactic extinction and inclination effect.
[b]Isophotal radius (25 mag arcsec^{-2} in the B band) corrected for Galactic extinction and absorption because of the inclination of NGC 628.

(Elmegreen et al. 2006). It is believed that turbulence plays a major role in star formation; it creates density enhancements that become gravitationally unstable and collapse to form stars (Elmegreen et al. 2006). The spatial distribution of young stars and stellar groups on wide length-scales probably reflects this process.

The purpose of this paper is to study the size distribution and hierarchical structures of star formation regions in the nearby face-on spiral galaxy NGC 628 (Fig. 1), based on our own observations in the U, B and V passbands. This galaxy is an excellent example of a galaxy with numerous star formation regions observed at different length-scales. We use the term 'star formation regions', which includes young star complexes, OB associations and H II regions (i.e. all young stellar groups regardless of their sizes).

Hodge (1976) identified 730 H II regions in the galaxy. Ivanov et al. (1992) estimated the sizes and magnitudes of 147 young stellar associations and aggregates in NGC 628 and discussed briefly hierarchical structures at scales from 50 to 800 pc. Larsen (1999) studied 38 young star clusters with effective diameters from 2 to 90 pc. Bruevich et al. (2007) obtained the magnitudes, colours and sizes of 186 star formation regions based on the list of H II regions from Belley & Roy (1992).

Elmegreen et al. (2006) studied the distributions of size and luminosity of star formation regions over a range of scales from 2 to 110 pc using progressively blurred versions of blue optical and Hα images from the *Hubble Space Telescope* (*HST*). They counted and measured features in each blurred image using the SEXTRACTOR program and found that the cumulative size distribution satisfies a power law with a slope of approximately −1.8 to −1.5 on all studied scales.

The fundamental parameters of NGC 628 are presented in Table 1. We take the distance to NGC 628, obtained by Sharina, Karachentsev & Tikhonov (1996) and van Dyk, Li & Filippenko (2006). We have used the position angle and the inclination of the galactic disc, derived by Sakhibov & Smirnov (2004). Other parameters were taken from the LEDA data base[1] (Paturel et al. 2003). We adopt the Hubble constant $H_0 = 75$ km s^{-1} Mpc^{-1} in the paper. With the assumed distance to NGC 628, we estimate a linear scale of 34.9 pc arcsec^{-1}.

Observations and reduction stages of *UBVRI* images for NGC 628 have already been published by Bruevich et al. (2007). The reduction of the photometric data was carried out using standard techniques, with the European Southern Observatory Munich Image Data Analysis System[2] (ESO-MIDAS).

2 IDENTIFICATION AND SIZE ESTIMATIONS OF STAR FORMATION REGIONS

Bruevich et al. (2007) have identified star formation regions in the galaxy using the list of H II regions of Belley & Roy (1992), based on their Hα spectrophotometric data. The list of Belley & Roy (1992) is still the most complete survey of H II regions and their parameters in NGC 628. Note that our coordinate grid coincides with that of Kennicutt & Hodge (1980) and is systematically shifted with respect to that of Belley & Roy (1992). Altogether, we have identified 127 of the 132 star formation regions studied by Belley & Roy (1992). Three regions (1, 2 and 96 in Belley & Roy 1992) were outside the field of view of our images. Two star formation regions (23 and 76) are missing in the list of Belley & Roy (1992). Belley & Roy (1992) did not distinguish between isolated star formation regions, with typical sizes of about 60–70 pc, and compound multicomponent regions, with typical sizes of about 200 pc. We obtained images of the galaxy with better seeing than Belley & Roy (1992). As a result, we have been able to resolve the compound star formation regions into components.

First, we identified such subcomponents by eye. We selected the components, the maximal (central) brightness in which was at least three times higher than the brightness of the surrounding background. Next, we fitted the profiles of the star formation regions using Gaussians. The separation condition of the components is that the full width at half-maximum (FWHM) of the region is less than the distance between the centres of Gaussians. The numbers of these complexes in the first column of Table A1 contain additional letters ('a', 'b', 'c' and 'd'). Compound regions that do not satisfy this condition are classified as objects with observed, but unresolved, internal structure. In total, we have identified 186 objects (Fig. 1).

In this paper, we use the numbering order adopted by Bruevich et al. (2007), which coincides with the numbering order of Belley & Roy (1992) with the exception of the missed star formation regions.

We have found that 146 regions from Table A1 have a star-like profile (see the last column in this table). Another 40 objects have a non-star-like – extended (diffuse) or multicomponent – profile (i.e. these objects have an observed, but unresolved, internal structure).

We took the geometric mean of major and minor axes of a star formation region for the star formation region's characteristic diameter d: $d = \sqrt{d_{\max} \times d_{\min}}$. We measured $d_{\max}$ and $d_{\min}$ from the radial V profiles as the FWHM for regions having a star-like profile, or as the distance between points of maximum flux gradient for regions having non-star-like profiles. We adopted seeing for the uncertainty in the size measurements, which definitely exceeds all other errors. The obtained parameters of the star formation regions are presented in Table A1.

3 HIERARCHICAL STRUCTURES OF STAR FORMATION REGIONS

The simplest way to study hierarchical clustering is to identify structures of different hierarchical levels, based on lower-level surface brightness thresholds above the background level. A similar method was used by Gouliermis et al. (2010), who used the stellar density

[1] http://leda.univ-lyon1.fr/

[2] http://www.eso.org/sci/software/esomidas/

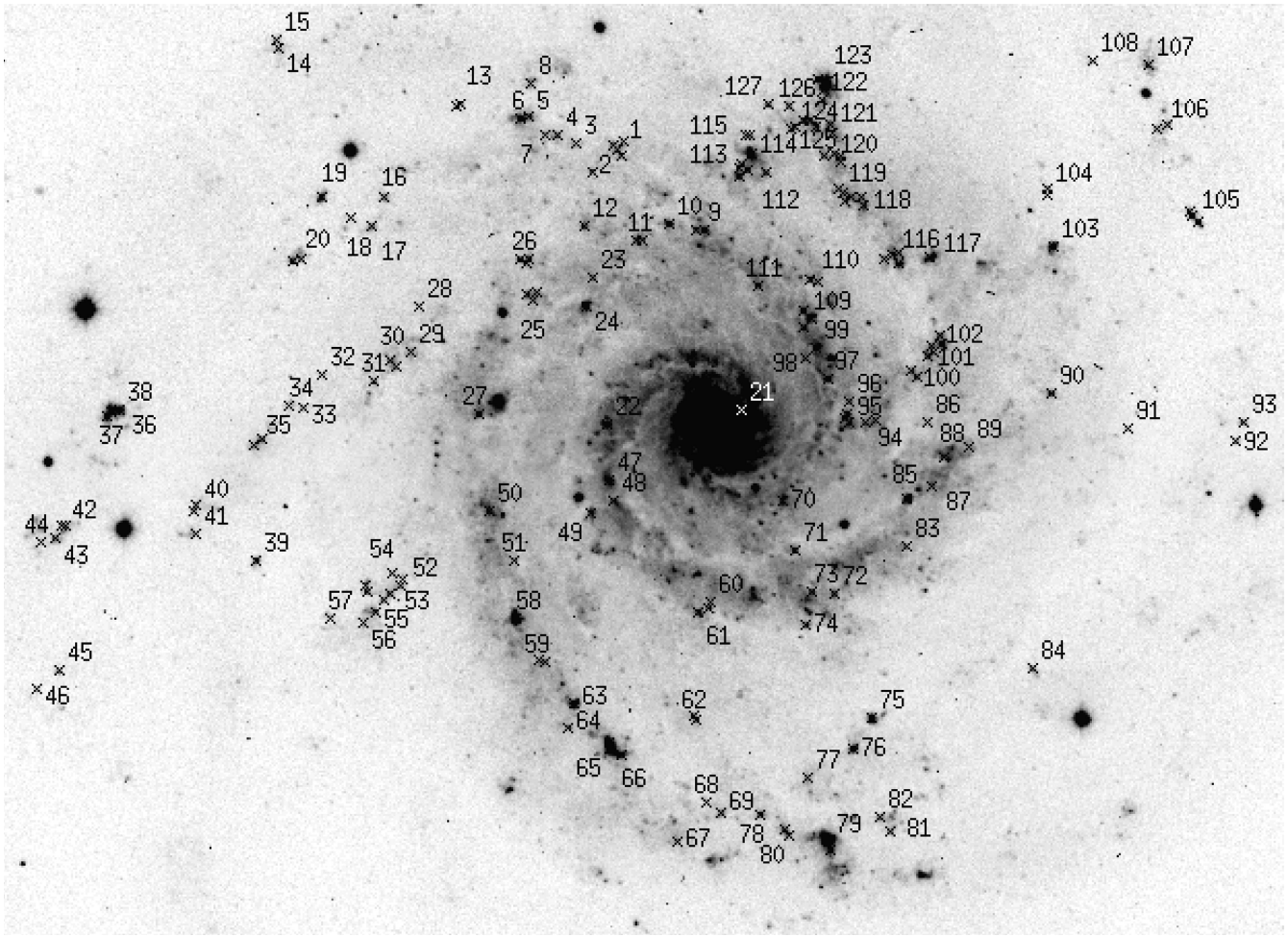

Figure 1. *B*-band image of NGC 628 and the positions of the galaxy's star formation regions (crosses). The numbers of the star formation regions from Table A1 are indicated. The image size is 8.26 × 6.00 arcmin. North is upward and east is to the left.

levels to study hierarchical stellar structures in the dwarf irregular galaxy NGC 6822. They identified hierarchical structures using density thresholds 1σ–5σ above the average background density level with a step of 1σ.

However, this direct way is not applicable for identification of hierarchical structures in NGC 628. The background level varies significantly in the galactic plane. The surface brightness of the background differs by several times inside spiral arms and in inter-arm regions.

Therefore, we have modified the technique of Gouliermis et al. (2010). The identification and size estimation of 186 star formation regions at the highest hierarchical level (level 1) were carried out using their half-maximum brightness levels, independent of background levels (see Section 2). Additionally, we fitted the profiles of star formation regions along their minor and major axes using Gaussians. To identify structures of level 2 and lower, we measured the background surface brightness in the *V* passband in the vicinity of every group of star formation regions of level 1.

The selection of a threshold in units of σ above the average brightness level of background for star formation regions of level 2 was carried out based on two basic conditions: (i) it must be lower than the level of brightness of the appropriate star formation region of level 1 and (ii) it must deviate more than four pixels (seeing of the *V* image) from the fitting Gaussian of the profile of the star formation region at level 1. The same conditions were applied to select the brightness level of every next lower level of the hierarchy. The exception was made for several resolved close binary star formation regions, such as 40a and 40b, where the second condition is not applied. To identify star formation regions of lower hierarchical levels, we used lower levels of brightness.

To select surface brightness thresholds, we first analysed a typical light distribution in selected star formation regions and their vicinities. Fig. 2 shows examples of such regions, star formation regions 33–35.

Fig. 2 (central panel) shows that the surface brightness falls irregularly with distance from the knots of star formation: 'plateau-like' areas with constant surface brightness alternate with areas of a sharp drop in brightness. At such sites, a fall in brightness usually exceeds the 1σ value. At higher hierarchical levels, where the surface brightness is higher, the absolute drop in brightness is larger than at lower levels of the hierarchy. As a result, the diameters of star formation regions increase slowly with a decrease of brightness level within the same hierarchical level. Significant growth of the diameters is observed only at the merger of two separate star formation regions into one common star formation region at the lower hierarchical level (Fig. 2).

We consider brightness in units of σ. So, the brightness level where the maximum brightness decrease is observed is also measured in units of σ. The maximum brightness decrease corresponds to the minimum of the first derivative of the brightness profile

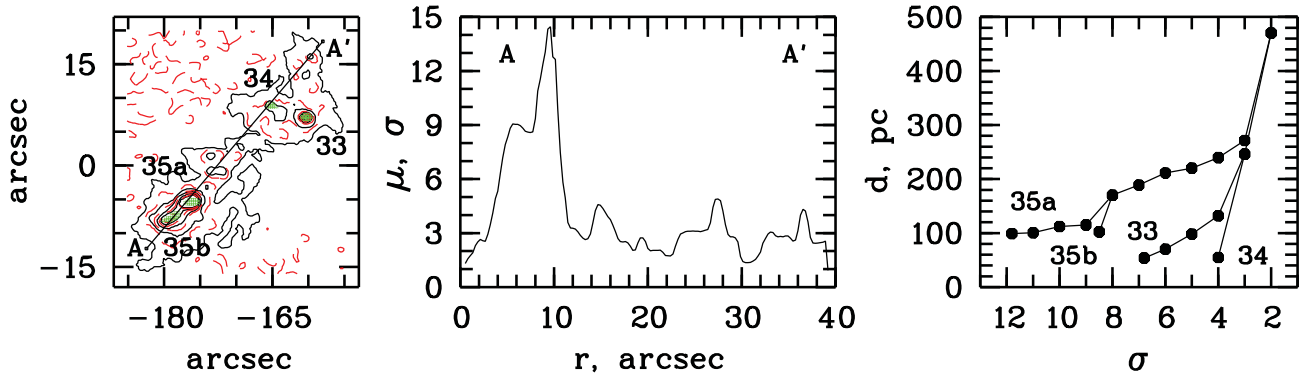

Figure 2. Left panel: contour map of the vicinity of star formation regions 33–35. Grey areas correspond to the regions 33, 34, 35a and 35b within their half-maximum brightness level. Red dashed contour levels correspond to the levels of σ, 3σ, 5σ, 7σ and 9σ, and black solid contour levels correspond to the levels of 2σ, 4σ, 6σ, 8σ and 10σ above the average brightness level of background. The position of profile A–A' is shown. Central panel: photometric profile A–A'. Surface brightness, μ, is given in units of σ. Right panel: diameters of star formation regions 33–35 and their hierarchical structures measured at the different levels of surface brightness in units of σ.

function (Fig. 2, central panel) in units of σ. After measuring the brightness level in units of σ by the maximum brightness decrease, we determine size of the star formation region with the isophots as described in Section 2.

We have analysed all the hierarchical structures in the vicinities of the star formation regions of level 1 and have determined which level of brightness corresponds to the level of maximum brightness decrease in these (Fig. 3).

The distribution of star formation regions of levels 2–5 by the level of maximum brightness decrease shows two maxima at 3σ and 5σ (Fig. 3). The distribution of star formation regions of the lowest hierarchical level has a maximum at 2σ–3σ, and the distribution of star formation regions of the first hierarchical level from the lowest level shows maxima at 3σ and 5σ–6σ. The star formation regions of the second hierarchical level from the lowest level have characteristic levels of maximum brightness decrease of 5σ, 8σ and 11σ (Fig. 3).

An analysis of the distribution of star formation regions by the level of maximum brightness decrease, in units of σ, has shown that neither arithmetic nor geometric sequences of the brightness levels are suitable to describe the hierarchical structures of star formation regions. When using a geometric sequence, we might miss some

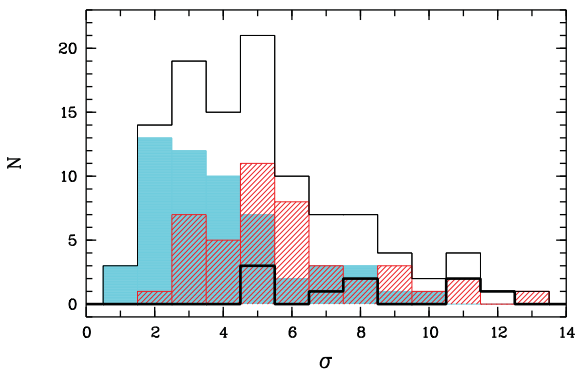

Figure 3. Distribution histogram of star formation regions of levels 2–5 by the level of maximum brightness decrease. Brightness is given in units of σ. The grey histogram is the distribution of star formation regions of the lowest hierarchical level. The shaded histogram is the distribution of star formation regions of the first hierarchical level from the lowest level. The thick black histogram is the distribution of star formation regions of the second hierarchical level from the lowest level. See the text for details.

of the hierarchical levels. When using an arithmetic sequence, we lose some of the brightness levels because they do not satisfy the condition (ii) (Fig. 2). In this case, low hierarchical levels will correspond to arbitrary levels of brightness.

An analysis of the distribution has shown that the best sequence of brightness levels is the Fibonacci sequence, 1σ, 2σ, 3σ, 5σ, 8σ, as an intermediate sequence between arithmetic and geometric sequences.

The diameters of the star formation regions of the lower hierarchical levels, which have the maximum brightness decrease at the level of 4σ or 6σ–7σ, are measured at the next lower surface brightness level of 3σ or 5σ, respectively. Typically, the difference between the diameters measured at the levels of 3σ and 4σ, or 5σ and 6σ–7σ does not exceed 35–40 pc, a value of the seeing of the image (Fig. 2).

Thus, we have used surface brightness thresholds of 8σ, 5σ, 3σ and 2σ above the average brightness level of background in the vicinity of the star formation region. The threshold of 1σ was not used because of large fluctuations of background around many identified groups of star formation regions.

For each individual region, not every next lower brightness level satisfies the conditions adopted. Such brightness levels have been missed. Furthermore, a full set of brightness levels from 8σ to 2σ above the background was used only for star formation regions 79a and 79b and hierarchical structures of a lower order related to these (Table A2). The lowest level of every hierarchical structure usually corresponds to the brightness level of 2σ or 3σ above the background (Fig. 3). As a result, the same hierarchical level might correspond to different levels of brightness.

The diameters of star formation regions at level 2 and lower were measured in the same manner as for star formation regions of level 1: $d = \sqrt{d_{\max} \times d_{\min}}$, where $d_{\min}$ and $d_{\max}$ are the diameters along the major and minor axes of the star formation region.

Table A2 presents the star formation regions obtained on different hierarchical levels, and their sizes. Some star formation regions of low hierarchical levels consist of one or several star-like cores (star formation regions of level 1) and an extended halo. Such star formation regions are indicated by the letter 'h' in Table A2. Fig. 4 shows a map of the locations of these objects in the galactic plane.

To illustrate the hierarchical structures, we have used so-called dendrograms. Dendrograms were introduced as 'structure trees' for the analysis of molecular cloud structures by Houlahan & Scalo (1992), they were refined by Rosolowsky et al. (2008), and they

were used by Gouliermis et al. (2010) to study hierarchical stellar structures in the nearby dwarf galaxy NGC 6822. A dendrogram is constructed by cutting an image at different brightnesses and identifying connected areas, while keeping track of the connection to surface brighter smaller structures (on a higher level) and surface fainter larger structures (on the next lower level, which combines structures of the previous level).

Fig. 5 presents the dendrogram for the star formation regions from Tables A1 and A2. Unlike Gouliermis et al. (2010), we constructed the dendrogram using the ordinate axis in units of diameter, which better illustrates the length-scales of the hierarchical structures. The combination of this dendrogram with the map of Fig. 4 illustrates graphically the hierarchical spatial distribution of the star formation regions in NGC 628.

The dendrogram demonstrates that most star formation regions are combined into larger structures over, at least, one to two levels. We found only 12 separate associations without a visible internal structure, which are out of hierarchical structures (Fig. 5). Most of these are located in the interarm regions (Fig. 1). The largest ($d > 1$ kpc) and the most populous (8–17 star formation regions of level 1) structures are located in the ends of the spiral arms. The first of these structures (75–80) is located near the corotation radius, which was obtained by Sakhibov & Smirnov (2004) based on a Fourier analysis of the spatial distribution of radial velocities of the gas in the disc of NGC 628. The largest – and brightest in ultraviolet – star complex of the galaxy was found here by Gusev, Egorov & Sakhibov (2014). The second structure (120–127) is located in the north-western part of NGC 628, in the disturbed part of the spiral arm (Fig. 1).

As seen from the dendrogram, the numbering order does not reflect correctly the hierarchical structures. The numbering is violated for star formation regions 4–7 at level 2, 85–89 at level 4 and 97–109 at level 4 (Table A2).

4 SIZE DISTRIBUTIONS OF STAR FORMATION REGIONS

Fig. 6 presents size distribution histograms for the three sets of star formation regions under study. The first set includes 297 regions of all hierarchical levels, the second set is a sample of 146 associations with a star-like profile and the third set includes 111 regions of level 2 and lower from Table A2. The second set unites the

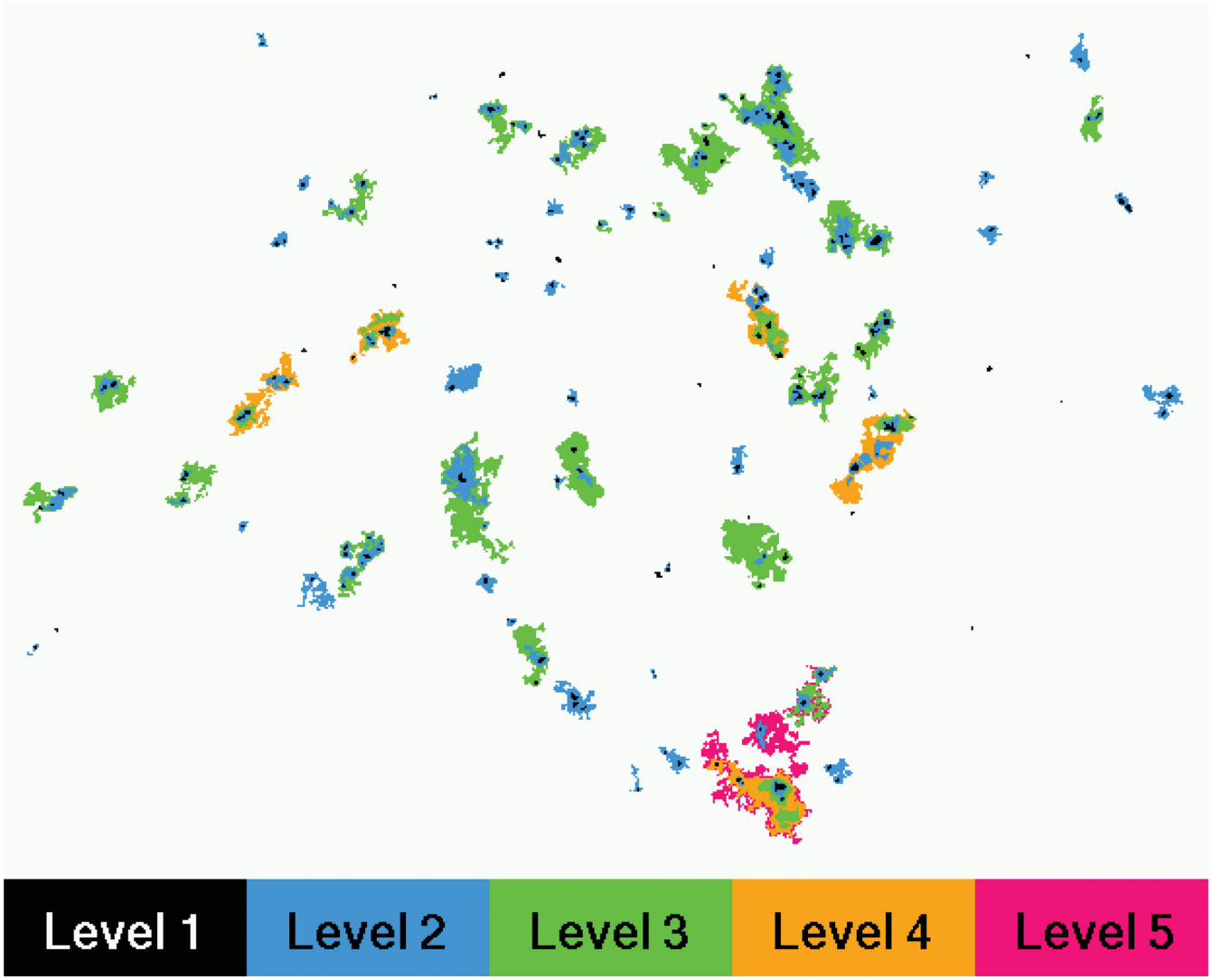

Figure 4. Map of star formation regions of different levels of the hierarchy. Regions of higher levels of the hierarchy are shaded darker than lower levels. The image size is 8.26 × 6.00 arcmin. North is upward and east is to the left.

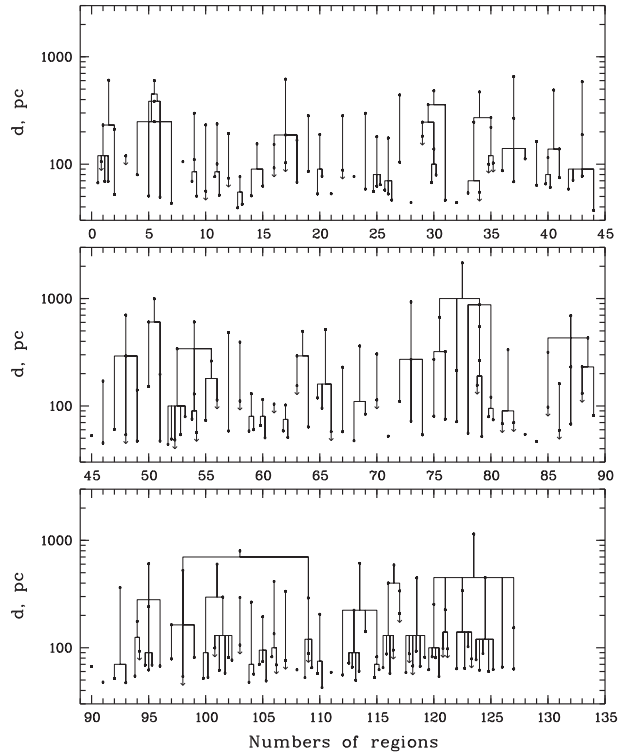

Figure 5. Dendrogram of the structures of the star formation regions. The black dots indicate star formation regions from Tables A1 and A2. Regions that are united into a hierarchical structure are connected by a solid line. The numbering order might not strictly follow the order of hierarchical structures (see the text for details). The arrows pointing down indicate star formation regions with an observed internal structure (star formation regions with a non-star-like profile).

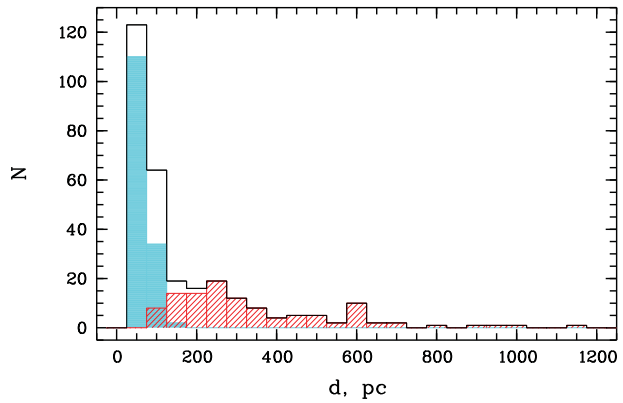

Figure 6. Number distribution histograms of all star formation regions from Tables A1 and A2, the star formation regions of level 1 with a star-like profile (grey histogram) and the star formation regions of level 2 and lower (shaded histogram).

star formation regions without an observed internal structure; their subcomponents (if they exist) have sizes ≤35–40 pc. The third set includes only star formation regions with obvious internal structure; their subcomponents have been detected and measured.

As seen from the figure, associations with a star-like profile have a narrow range of sizes, from 40 to 100 pc, with a few exceptions. The mean diameter of these star formation regions is equal to 66 ± 18 pc. This is a typical size for OB associations. The star formation regions with an extended profile have, on average, slightly larger sizes, ∼100 pc. As a result, the size distribution of star formation regions of level 1 with both star-like and extended profiles is displaced a little towards the larger sizes (see Fig. 6 and Table 2).

Table 2. Diameters of star formation regions.

Star formation regions	d^a (pc)	d^b (pc)
Associations[c]	66 ± 18	64
Associations[d]	72 ± 26	66
Aggregates	240 ± 90	234
Complexes	583 ± 84	601

[a] Mean diameter.
[b] Diameter obtained from best-fitting Gaussian.
[c] Associations with a star-like profile (146 objects).
[d] All associations from Table A1 (186 objects).

The star formation regions of lower levels clearly show a bimodal size distribution. Two maxima at ≈250 and ≈600 pc are observed (Fig. 6). The first smoothed peak corresponds to a characteristic size of stellar aggregates by the classification of Efremov et al. (1987), and the second peak is located on the diameters, which are typical for star complexes.

We also fitted size distributions of the studied sets of star formation regions using Gaussians. To fit the size distribution for the set of 111 complex star formation regions, we used a combination of two Gaussians. It was found that all sets of star formation regions have size distributions close to the Gaussian distribution. The diameters obtained from the best-fitting Gaussians are almost the same as the mean diameters for all sets of star formation regions (Table 2).

Following Elmegreen et al. (2006), we constrained the cumulative size distribution function in the form $N(d > D) \propto D^{\gamma}$, where N is the integrated number of objects that have a diameter d greater than some diameter D (Fig. 7).

A detailed exploration of the size distribution of objects in NGC 628 was carried out by Elmegreen et al. (2006) in the range of scales from 2 to 110 pc[3] based on *HST* images. For regions in the central part of the galaxy brighter than the 3σ noise limits in B and V images, Elmegreen et al. (2006) found that the cumulative size distribution obeys a power law, with a slope $\gamma \approx -1.5$ in the range 2–55 pc. A similar slope of the cumulative size distribution function was found for OB associations from the list of Ivanov et al. (1992) in the range 30–110 pc. The size distribution of larger objects, H II regions studied by Hodge (1976), satisfies a power law with a slope $\gamma \approx -3.5$ in the range 100–300 pc. The size distribution of large star formation regions (in the range 300–600 pc) in the spiral arms of NGC 628 obtained by Gusev et al. (2014) shows a slope $\gamma \approx -4.5$. The size distribution of complexes from Ivanov et al. (1992) gives $\gamma = -4.1$ in the range 500–1000 pc (Fig. 7).

Summarizing the results of the size distribution obtained previously, we can conclude that the size distributions of star formation regions with a diameter of ≤100 pc satisfy a power law with $\gamma \approx -1.5$. The distribution of larger star formation regions obeys a power law with γ between ≈− 5 and ≈− 3.5.

Fig. 7 (right panel) presents size distribution functions constructed for three sets of star formation regions. The first set includes

[3] For an adopted distance of 7.2 Mpc.

297 regions of all hierarchical levels, the second set is a sample of 186 star formation regions of level 1 and the third set includes 146 regions of level 1 with a star-like profile.

The size distribution of 146 star formation regions with a star-like profile, beginning with $d \approx 50$ pc, obeys a power law with a slope $\gamma \approx -5$. The size distribution of all 186 star formation regions of level 1 satisfies a power law with a slope $-4 \leq \gamma \leq -3.5$ in the range 50–170 pc. It repeats the distribution of H II regions of Hodge (1976) with a displacement $\log D \approx 0.2$ (Fig. 7). In general, the size distribution of star formation regions of level 1 has slopes between -5 and -3.5, like the size distributions of previously studied star formation regions of a single level of hierarchy (Fig. 7).

Note, that the end of the size distribution curve for the regions of Elmegreen et al. (2006) coincides with the beginning of the size distribution curve for our 186 star formation regions of level 1 (Fig. 7). Given that the area studied by Elmegreen et al. (2006) occupies ∼70 per cent of the area of NGC 628, which is studied in this paper, we can conclude that (i) the number of H II regions identified by Belley & Roy (1992) is smaller than the numbers of regions found by Elmegreen et al. (2006) using SEXTRACTOR and, which is more important, (ii) our measurements of the sizes of star formation regions using photometric profiles are in good agreement with the measurements of Elmegreen et al. (2006).

More interesting behaviour is observed for the curve of the size distribution of star formation regions of all hierarchical levels. It continues the size distribution curve for regions of Elmegreen et al. (2006) at $d = 30$–40 pc and has the same slope ≈ -1.5 in the range 45–85 pc – diameters of OB associations. A flatter slope, $\gamma > -1$, is observed in the range from ≈90 to ≈180 pc for regions of level 1 with an extended profile and for the smallest regions of level 2. The size distribution of star formation regions, which are classified as stellar aggregates and complexes, obeys a power law with $\gamma = -1.5$ very well (see the distribution curve in the range 190–600 pc in Fig. 7). The largest hierarchical structures with $d = 0.65$–0.9 kpc are also distributed by sizes by a power law with $\gamma \sim -1.5$ (Fig. 7).

Thus, the size distribution of the star formation regions of all hierarchical levels continues the size distribution function for regions of Elmegreen et al. (2006) towards the larger sizes with the same slope ≈ -1.5.

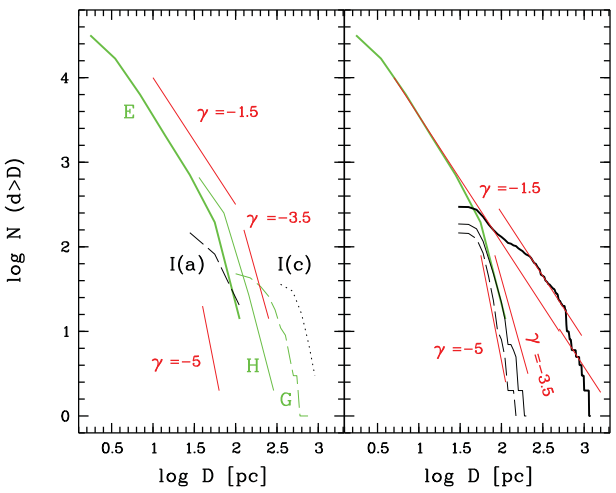

Figure 7. Left panel: cumulative size distribution functions for regions of Elmegreen et al. (2006) (E, grey thick solid curve), H II regions of Hodge (1976) (H, grey thin solid curve), associations [I(a), black dashed curve] and complexes [I(c), black dotted curve] of Ivanov et al. (1992), and large star formation regions in the spiral arms of the galaxy (G, grey thin dashed curve) from Gusev et al. (2014). Right panel: cumulative size distribution functions for regions of Elmegreen et al. (2006) (grey thick solid curve), 146 star formation regions with a star-like profile from Table A1 (black dashed curve), 186 star formation regions from Table A1 (black solid curve), and 297 star formation regions from Tables A1 and A2 (black thick curve). The dark thin solid straight lines in both panels represent slopes $\gamma = -1.5$, -3.5 and -5 of the size distribution function. See the text for details.

5 DISCUSSION

The modern theory of star formation explains the existence of OB associations and star complexes, which are associated by unity of an origin with hydrogen superclouds and giant molecular clouds, respectively (Elmegreen & Efremov 1996; Efremov & Elmegreen 1998). Structures of H_2 on the intermediate scalelength are unknown. However, such intermediate young stellar structures are observed in galaxies. These are stellar aggregates with diameters ∼200–300 pc.

Fig. 6 shows a bimodal size distribution of star formation regions of level 2 and lower. Bimodal size distributions with a secondary peak at $d = 150$–300 pc were found for 'associations' in the Small Magellanic Cloud (Battinelli 1991), M31 (Magnier et al. 1993), NGC 2090, 2541, 3351, 3621 and 4548 (Bresolin et al. 1998), NGC 1058 and UGC 12732 (Battinelli et al. 2000), NGC 300 (Pietrzyński et al. 2001), NGC 3507 and 4394 (Vicari et al. 2002), and NGC 7793 (Pietrzyński et al. 2005). Pietrzyński et al. (2005) called such associations 'superassociations'.

Thus, the existence of stellar structures, aggregates or superassociations, with a characteristic size 200–300 pc, is confirmed by numerous observations in different galaxies. However, the question concerning the origin of stellar aggregates is still open.

As we have noted above, the size distribution of star formation regions of all hierarchical levels continues the size distribution of regions of Elmegreen et al. (2006) with the same slope ≈ -1.5 for sizes from 45 pc to ∼0.9 kpc. However, the size distribution function deviates from a power law with the slope -1.5 at $d = 90$–180 pc and 600–650 pc (Fig. 7).

We believe that the flatter slope in the range 90–180 pc is a result of significant number of star formation regions with a diameter of ∼100–150 pc with an unresolved internal structure. Taking into account such undetected objects will shift the distribution curve upward along the ordinate axis at sizes smaller than or equal to the diameters of these star formation regions.

The opposite situation is observed at $d = 600$–650 pc. The largest structures with $d > 600$ pc have a low boundary surface brightness. They are difficult to identify in the spiral arms of the grand design galaxy NGC 628 because of the significant variations of background level (see Section 4). The underestimation of the number of star formation regions at the lowest hierarchical levels leads to a drastic drop in the size distribution curve.

In spite of small statistics, the largest star formation regions with $d \approx 0.65$–0.9 kpc are also distributed by size by a power law with $\gamma \sim -1.5$. This can be an additional argument in favour of the assumption of Efremov et al. (1987), Elmegreen & Efremov (1996) and Zhang et al. (2001), who assumed that the hierarchical structures extend to the scale of 1 kpc.

It is crucial for the construction of the cumulative size distribution function to take into account the hierarchy of star formation regions. Neglecting the internal structure of star formation regions of higher hierarchical levels and underestimating the number of star formation regions of lower hierarchical levels lead to a decrease or an increase of the slope of the size distribution function,

respectively. To illustrate this, in Fig. 7, we compare the size distributions of the regions of Elmegreen et al. (2006), our star formation regions of all hierarchical levels and our star formation regions of level 1 with any profiles in the range of scale from 50 to 110 pc.

On the scale of 200–600 pc, the characteristic sizes of stellar aggregates and complexes, the size distribution function has a constant slope. We believe that the sample of objects at the different levels of hierarchy within this scale range is complete.

The slope γ of the cumulative size distribution function for star formation regions is of fundamental importance. It is associated with the fractal dimension of objects in the galaxy at different scales. Elmegreen et al. (2006) introduced the fractal of dimension $\mathcal{D}$, where $\mathcal{D} = -\gamma$. Following Elmegreen et al. (2006), we believe that the size distribution of stellar groups suggests a fractal distribution of stellar positions projected on the disc of the galaxy, with a constant fractal dimension of $\mathcal{D} \approx 1.5$ in the wide range of length-scales from 2 pc to 1 kpc. It is comparable to the fractal dimension of projected local interstellar clouds, $\mathcal{D} \approx 1.3$ (Falgarone, Phillips & Walker 1991), and to the fractal dimension of H I ($\mathcal{D} = 1.2$–1.5) in the M81 group of galaxies (Westpfahl et al. 1999).

6 CONCLUSIONS

We have studied the hierarchical structures and the size distribution of star formation regions in the spiral galaxy NGC 628 over a range of scales from 50 to 1000 pc based on the size estimations of 297 star formation regions. Most star formation regions are combined into larger structures over several levels. We have found three characteristic sizes of young star groups: OB associations with mean diameter $d = 66 \pm 18$ pc, stellar aggregates ($d = 240 \pm 90$ pc) and star complexes (583 ± 84 pc).

The cumulative size distribution function of star formation regions satisfies a power law with a slope of -1.5 at scales from 45 to 85 pc, from 190 to 600 pc, and from 650 pc to 900 pc, which are appropriate to the sizes of associations, aggregates and complexes. Together with the result of Elmegreen et al. (2006), who found the slope $-1.8 \leq \gamma \leq -1.5$ for regions at scales from 2 to 100 pc, our result shows that the size distribution of young stellar structures in the galaxy obeys a power law with a constant slope of ≈ -1.5 at all studied scales from $\approx$2 pc to $\approx$1 kpc.

Ignoring the hierarchical structures (i.e. using star formation regions of only one hierarchical level to examine the size distribution) gives slopes $-5 \leq \gamma \leq -3$.

ACKNOWLEDGEMENTS

I am grateful to the referee for constructive comments, and to Yu. N. Efremov (Sternberg Astronomical Institute) for useful discussions. I would like to thank E. V. Shimanovskaya (Sternberg Astronomical Institute) for help with editing this paper. I acknowledge the use of the HyperLeda data base (http://leda.univ-lyon1.fr). This study was supported in part by the Russian Foundation for Basic Research (project nos. 12–02–00827 and 14–02–01274).

REFERENCES

Ballesteros-Paredes J., Klessen R. S., MacLow M.-M., Vazquez-Semadeni E., 2007, in Reipurth B., Jewitt D., Keil K., eds, Protostars and Planets V. Univ. of Arizona Press, Tucson, p. 63
Bastian N., Gieles M., Efremov Yu. N., Lamers H. J. G. L. M., 2005, A&A, 443, 79
Battinelli P., 1991, A&A, 244, 69
Battinelli P., Efremov Y., Magnier E. A., 1996, A&A, 314, 51
Battinelli P., Capuzzo-Dolcetta R., Hodge P. W., Vicari A., Wyder T. K., 2000, A&A, 357, 437
Belley J., Roy J.-R., 1992, ApJS, 78, 61
Bianchi L., Efremova B., Hodge P., Kang Y., 2012, AJ, 144, 142
Borissova J., Kurtev R., Georgiev L., Rosado M., 2004, A&A, 413, 889
Brandeker A., Jayawardhana R., Najita J., 2003, AJ, 126, 2009
Bresolin F., Kennicutt R. C. Jr, Stetson P. B., 1996, AJ, 112, 1009
Bresolin F. et al., 1998, AJ, 116, 119
Bruevich V. V., Gusev A. S., Ezhkova O. V., Sakhibov F. Kh., Smirnov M. A., 2007, Astron. Rep., 51, 222
Bruevich V. V., Gusev A. S., Guslyakova S. A., 2011, Astron. Rep., 55, 310
Dahm S. E., Simon T., 2005, AJ, 129, 829
de la Fuente Marcos R., de la Fuente Marcos C., 2009, ApJ, 700, 436
Efremov Yu. N., 1989, Sites of Star Formation in Galaxies: Star Complexes and Spiral Arms. Fizmatlit, Moscow, p. 246 (in Russian)
Efremov Yu. N., 1995, AJ, 110, 2757
Efremov Yu. N., Elmegreen B. G., 1998, MNRAS, 299, 588
Efremov Yu. N., Ivanov G. R., Nikolov N. S., 1987, Ap&SS, 135, 119
Elmegreen B. G., 1994, ApJ, 433, 39
Elmegreen B. G., 2002, ApJ, 564, 773
Elmegreen B. G., 2006, in Del Toro Iniesta J. C., Alfaro E. J., Gorgas J. G., Salvador-Sole E., Butcher H., eds, The Many Scales in the Universe: JENAM 2004 Astrophysics Reviews. Springer, Dordrecht, p. 99
Elmegreen B. G., 2009, in Andersen J., Bland-Hawthorn J., Nordström B., eds, Proc. IAU Symp. 254, The Galaxy Disk in Cosmological Context. Kluwer, Dordrecht, p. 289
Elmegreen B. G., 2011, in Charbonnel C., Montmerle T., eds, in EAS SP-51, Ecole Evry Schatzman 2010: Star Formation in the Local Universe. Cambridge Univ. Press, Cambridge, p. 31
Elmegreen B. G., Efremov Yu. N., 1996, ApJ, 466, 802
Elmegreen B. G., Elmegreen D. M., 2001, AJ, 121, 1507
Elmegreen B. G., Efremov Y., Pudritz R. E., Zinnecker H., 2000, in Mannings V., Boss A. P., Russell S. S., eds, Protostars and Planets IV. Univ. of Arizona Press, Tucson, p. 179
Elmegreen B. G., Elmegreen D. M., Leitner S. N., 2003a, ApJ, 590, 271
Elmegreen B. G., Leitner S. N., Elmegreen D. M., Cuillandre J.-C., 2003b, ApJ, 593, 333
Elmegreen B. G., Elmegreen D. M., Chandar R., Whitmore B., Regan M., 2006, ApJ, 644, 879
Falgarone E., Phillips T., Walker C. K., 1991, ApJ, 378, 186
Feitzinger J. V., Braunsfurth E., 1984, A&A, 139, 104
Gouliermis D. A., Schmeja S., Klessen R. S., de Blok W. J. G., Walter F., 2010, ApJ, 725, 1717
Gusev A. S., 2002, Astron. Astrophys. Trans., 21, 75
Gusev A. S., Egorov O. V., Sakhibov F., 2014, MNRAS, 437, 1337
Harris J., Zaritsky D., 1999, AJ, 117, 2831
Heydari-Malayeri M., Charmandaris V., Deharveng L., Rosa M. R., Schaerer D., Zinnecker H., 2001, A&A, 372, 495
Hodge P. W., 1976, ApJ, 205, 728
Houlahan P., Scalo J., 1992, ApJ, 393, 172
Ivanov G. R., 1991, Ap&SS, 178, 227
Ivanov G. R., Popravko G., Efremov Y. N., Tichonov N. A., Karachentsev I. D., 1992, A&AS, 96, 645
Kennicutt R. C., Hodge P. W., 1980, ApJ, 241, 573
Krumholz M. R., McKee C. F., 2005, ApJ, 630, 250
Kumar M. S. N., Kamath U. S., Davis C. J., 2004, MNRAS, 353, 1025
Larsen S. S., 1999, A&AS, 139, 393
Larson R. B., 1981, MNRAS, 194, 809
Magnier E. A. et al., 1993, A&A, 278, 36
Odekon M. C., 2008, ApJ, 681, 1248
Oey M. S., Watson A. M., Kern K., Walth G. L., 2005, AJ, 129, 393
Paturel G., Petit C., Prugniel Ph., Theureau G., Rousseau J., Brouty M., Dubois P., Cambresy L., 2003, A&A, 412, 45
Pietrzyński G., Gieren W., Fouqué P., Pont F., 2001, A&A, 371, 497
Pietrzyński G., Ulaczyk K., Gieren W., Bresolin F., Kudritzki R. P., 2005, A&A, 440, 783

Rosolowsky E. W., Pineda J. E., Kauffmann J., Goodman A. A., 2008, ApJ, 679, 1338
Sakhibov F. Kh., Smirnov M. A., 2004, Astron. Rep., 48, 995
Sánchez N., Añez N., Alfaro E. J., Crone Odekon M., 2010, ApJ, 720, 541
Sánchez-Monge Á. et al., 2013, MNRAS, 432, 3288
Sharina M. E., Karachentsev I. D., Tikhonov N. A., 1996, A&AS, 119, 499
van Dyk S. D., Li W., Filippenko A. V., 2006, PASP, 118, 351
Vicari A., Battinelli P., Capuzzo-Dolcetta R., Wyder T. K., Arrabito G., 2002, A&A, 384, 24
Westpfahl D. J., Coleman P. H., Alexander J., Tongue T., 1999, AJ, 117, 868
Wilson C. D., 1991, AJ, 101, 1663
Wilson C. D., 1992, ApJ, 386, L29
Zhang Q., Fall S. M., Whitmore B. C., 2001, ApJ, 561, 727

APPENDIX A: PARAMETERS AND HIERARCHICAL STRUCTURES OF STAR FORMATION REGIONS

Table A1. Identification, offsets, and diameters of star formation regions.

ID	ID (BR)[a]	N–S[b] (arcsec)	E–W[b] (arcsec)	*d* (pc)	Note[c]
1a	3	+108.8	−40.3	65	st
1b	3	+106.9	−38.5	105	
1c	3	+104.2	−37.4	70	st
1d	3	+110.4	−36.6	70	st
2	4	+98.4	−48.6	50	st
3	5	+109.0	−54.5	120	
4	6	+112.2	−61.9	80	st
5	7	+119.7	−72.9	50	st
6	8	+119.2	−76.1	50	st
7	9	+112.8	−67.0	45	st
8	10	+132.8	−72.3	105	st
9a	11	+75.5	−4.9	70	st
9b	11	+76.0	−8.6	50	st
10	12	+78.1	−18.7	55	
11a	13	+71.7	−31.3	75	st
11b	13	+72.0	−28.9	50	st
12	14	+77.1	−51.5	75	
13a	15	+124.0	−101.1	40	st
13b	15	+124.2	−99.3	40	st
14	16	+145.8	−170.2	50	st
15	17	+149.3	−170.7	65	st
16	18	+88.3	−128.9	90	
17	19	+77.3	−133.7	105	
18	20	+80.3	−141.9	70	st
19	21	+88.8	−153.1	85	st
20a	22	+63.7	−164.6	55	st
20b	22	+64.8	−161.4	75	st
21	24	+5.8	+9.5	55	st
22	25	+0.2	−43.0	90	
23	26	+57.6	−48.6	75	st
24	27	+46.1	−51.0	60	st
25a	28	+50.9	−73.7	55	st
25b	28	+51.4	−69.9	60	st
25c	28	+48.8	−71.3	65	st
26a	29	+64.2	−76.6	55	st
26b	29	+64.8	−73.4	55	st
26c	29	+62.6	−73.7	45	st
27	30	+4.5	−92.3	105	st
28	31	+46.4	−115.8	45	st
29	32	+28.5	−118.5	180	
30a	33	+25.0	−126.7	65	st
30b	33	+22.9	−124.6	80	st

Table A1 – *continued*

ID	ID (BR)[a]	N–S[b] (arcsec)	E–W[b] (arcsec)	*d* (pc)	Note[c]
31	34	+17.0	−133.1	45	st
32	35	+19.7	−153.1	45	st
33	36	+6.9	−160.3	55	st
34	37	+8.0	−165.7	55	
35a	38	−5.1	−176.1	100	
35b	38	−7.8	−179.3	100	
36	39	+3.7	−236.6	85	st
37	40	+5.0	−235.0	70	st
38	41	+6.1	−231.5	110	st
39	42	−52.3	−178.5	65	st
40a	43	−30.7	−201.9	65	st
40b	43	−33.1	−202.7	60	st
41	44	−41.9	−201.9	75	st
42a	45	−38.4	−253.9	60	st
42b	45	−39.0	−252.6	70	st
43	46	−43.8	−256.6	75	st
44	47	−45.1	−261.9	35	st
45	48	−95.0	−255.0	55	st
46	49	−102.2	−263.8	45	st
47	50	−21.1	−41.9	60	st
48	51	−29.1	−40.1	55	
49	52	−33.6	−48.9	45	st
50	53	−32.8	−88.3	150	st
51	54	−52.3	−78.5	45	st
52a	55	−57.1	−126.2	45	st
52b	55	−62.2	−122.7	50	st
52c	55	−59.5	−121.7	50	
53a	56	−67.5	−129.4	55	st
53b	56	−64.8	−127.0	80	st
54a	57	−64.3	−135.8	75	st
54b	57	−61.6	−136.3	55	
55	58	−72.0	−132.6	75	st
56	59	−76.6	−136.9	115	
57	60	−74.4	−149.9	60	st
58	61	−74.4	−77.9	110	
59a	62	−91.0	−68.9	60	st
59b	62	−91.5	−67.0	60	st
60a	63	−70.7	−3.3	65	st
60b	63	−68.6	−2.7	50	st
61	64	−72.6	−7.3	105	
62a	65	−112.3	−9.4	60	st
62b	65	−114.2	−8.6	50	st
63	66	−107.8	−55.5	155	
64	67	−116.8	−57.7	65	st
65a	68	−122.4	−42.2	120	st
65b	68	−125.4	−41.7	95	st
66	69	−127.2	−37.4	60	
67	70	−160.8	−15.8	60	st
68	71	−145.6	−4.6	45	st
69	72	−149.9	+1.3	85	st
70	73	−28.8	+25.3	115	
71	74	−48.3	+29.8	50	st
72	75	−65.4	+45.0	110	st
73	77	−64.3	+36.5	70	st
74	78	−77.1	+34.3	55	st
75	79	−113.4	+59.7	80	st
76	80	−125.1	+52.5	75	st
77	81	−136.6	+34.6	70	st
78	82	−150.4	+16.7	55	st
79a	83	−160.0	+42.6	155	
79b	83	−164.6	+43.9	50	st
80a	84	−156.6	+25.8	80	st
80b	84	−158.4	+27.4	75	st

Table A1 – *continued*

ID	ID (BR)[a]	N–S[b] (arcsec)	E–W[b] (arcsec)	*d* (pc)	Note[c]
81	85	−157.1	+66.9	70	
82	86	−151.8	+63.1	70	
83	87	−47.0	+73.0	55	st
84	88	−94.2	+121.8	45	st
85	89	−28.3	+73.5	95	
86	90	+1.6	+81.0	60	
87	91	−23.2	+82.9	70	st
88	92	−12.0	+87.7	130	
89	93	−8.0	+97.5	80	st
90	94	+12.5	+129.0	65	st
91	95	−1.4	+158.9	50	st
92	97	−6.2	+200.7	50	st
93	98	+1.3	+203.4	45	st
94a	99	+1.0	+57.0	55	st
94b	99	+2.1	+61.0	95	
95a	100	+1.0	+51.1	70	st
95b	100	+3.2	+49.3	60	st
95c	100	+4.8	+50.1	70	st
96	101	+9.6	+51.1	70	st
97	102	+17.8	+42.9	80	st
98	103	+25.8	+33.8	55	
99	104	+30.4	+38.3	80	st
100a	105	+21.0	+75.1	50	st
100b	105	+18.9	+77.0	55	st
101a	106	+27.2	+81.0	100	
101b	106	+28.2	+83.4	60	st
102a	107	+30.6	+82.9	60	st
102b	107	+31.7	+86.9	80	st
102c	107	+34.9	+86.1	75	st
103	108	+69.0	+129.8	105	
104a	109	+89.6	+127.7	50	st
104b	109	+92.0	+127.7	55	st
105a	110	+78.6	+186.1	70	st
105b	110	+81.1	+183.4	75	st
105c	110	+83.2	+182.9	50	st
106a	111	+115.2	+170.3	80	st
106b	111	+116.8	+174.3	70	
107	112	+139.4	+166.6	75	
108	113	+141.0	+145.0	60	st
109a	114	+37.8	+33.5	55	st
109b	114	+41.6	+36.2	90	
109c	114	+44.2	+33.0	65	st
110a	115	+56.8	+35.9	60	st
110b	115	+56.0	+38.6	45	st
111	116	+54.4	+15.7	60	st
112	117	+98.1	+18.6	55	st
113a	118	+96.5	+8.2	70	st
113b	118	+99.7	+8.2	65	st
113c	118	+101.3	+9.3	50	st
113d	118	+99.2	+11.4	60	st
114	119	+105.0	+13.0	140	st
115a	120	+112.2	+11.1	55	st
115b	120	+112.2	+12.5	65	st
116a	121	+64.8	+64.5	65	st
116b	121	+66.1	+67.5	90	st
116c	121	+66.9	+70.3	60	st
116d	121	+62.6	+70.3	95	
117	122	+65.3	+82.3	210	
118a	123	+87.2	+49.5	60	st
118b	123	+88.5	+51.4	90	
118c	123	+88.2	+55.4	70	
118d	123	+85.0	+56.7	95	st

Table A1 – *continued*

ID	ID (BR)[a]	N–S[b] (arcsec)	E–W[b] (arcsec)	*d* (pc)	Note[c]
119a	124	+90.1	+48.7	65	st
119b	124	+91.7	+46.9	80	st
120a	125	+104.2	+41.0	60	st
120b	125	+105.3	+45.5	80	st
120c	125	+104.2	+47.7	80	st
120d	125	+102.4	+47.4	55	st
121a	126	+113.3	+44.5	100	
121b	126	+116.8	+43.7	100	
122	127	+125.8	+40.7	65	st
123a	128	+134.1	+38.6	65	st
123b	128	+133.3	+42.1	100	st
123c	128	+130.4	+41.5	80	
124a	129	+118.1	+33.3	75	st
124b	129	+117.8	+35.9	60	st
124c	129	+116.0	+38.3	90	st
125a	130	+114.6	+28.2	60	st
125b	130	+115.7	+29.8	65	st
126	131	+123.7	+27.4	65	st
127	132	+124.2	+19.7	65	st

[a]ID number taken from Belley & Roy (1992).
[b]Offsets from the galactic centre, positive to the north and west.
[c]The abbreviation 'st' denotes a star-like profile.

Table A2. Hierarchical structures of star formation regions.

Level 1	Level 2	Level 3	Level 4	Level 5
1a–d	1 (230)[a]	1,2 (605)		
2	2h[b] (210)			
3				
4	4,7 (250)	4–7 (600)		
5	5,6 (385)			
6				
7				
8				
9a,b	9 (110)	9h (300)		
10	10h (230)			
11a,b	11 (100)	11h (235)		
12	12h (195)			
13a,b	13 (75)			
14	14,15 (155)			
15				
16	16h (155)	16–18 (620)		
17	17h (185)			
18	18h (165)			
19	19h (280)			
20a,b	20 (200)			
21				
22	22h (280)			
23				
24	24h (300)			
25a–c	25 (180)			
26a–c	26 (175)			
27	27h (440)			
28				
29	29h (245)	29,30 (360)	29–31	
30a,b	30 (140)		(480)	
31				
32				
33	33,34 (245)		33–35	
34			(470)	

Table A2 – *continued*

Level 1	Level 2	Level 3	Level 4	Level 5
35a,b	35 (220)	35h (270)		
36	36–38 (270)	36–38h (655)		
37				
38				
39	39h (165)			
40a,b	40 (115)	40,41 (490)		
41	41h (140)			
42a,b	42–44 (190)	42–44h (585)		
43				
44				
45				
46	46h (170)			
47		47–49 (700)		
48	48h (290)			
49	49h (140)			
50	50h (605)	50,51 (995)		
51	51h (195)			
52a–c	52,53 (340)	52–56 (605)		
53a,b				
54a,b	54 (130)			
55	55,56 (260)			
56				
57	57h (485)			
58	58h (395)			
59a,b	59 (130)			
60a,b	60 (115)			
61				
62a,b	62 (100)			
63	63h (290)	63,64 (495)		
64				
65a,b	65,66 (515)			
66				
67	67h (230)			
68	68,69 (360)			
69				
70	70h (305)			
71				
72		72–74 (930)		
73	73h (270)			
74				
75	75h (270)	75,76 (670)		75–80
76	76h (320)			(2150)
77	77h (215)			
78			78–80	
79a,b	79 (265)	79h (545)	(875)	
80a,b	80 (120)			
81	81,82 (335)			
82				
83				
84				
85	85h (315)		85,87–89 (695)	
86	86h (160)			
87	87h (230)			
88	88h (230)	88,89 (430)		
89				
90				
91				
92	92,93 (365)			
93				
94a,b	94 (175)	94–96 (605)		
95a–c	95 (240)			
96				
97	97h (165)	97–99 (525)	97–99,	
98			109 (800)	
99				
100a,b		100–102 (600)		
101a,b	101,102 (295)			
102a–c				
103	103h (295)			
104a,b	104 (265)			
105a–c	105 (195)			
106a,b	106 (135)	106h (415)		
107	107h (335)			
108				
109a–c	109 (290)			
110a,b	110 (205)			
111				
112		112–115 (610)		
113a–d	113 (225)			
114				
115a,b	115 (80)			
116a–d	116 (400)	116,117 (590)		
117	117h (340)			
118a–d	118,119 (445)			
119a,b				
120a–d	120 (255)	120–127 (1145)		
121a,b	121 (225)			
122	122,123 (340)			
123a–c				
124a–c	124,125 (450)			
125a,b				
126				
127	127h (155)			

[a] Diameter.
[b] Star formation region with halo.

This paper has been typeset from a TEX/LATEX file prepared by the author.